energies

MDPI

Article

Thin-Film Photovoltaic Modules Characterisation Based on *I-V* Measurements Under Outdoor Conditions

Slawomir Gulkowski * and Ewelina Krawczak

Department of Renewable Energy Engineering, Faculty of Environmental Engineering, Lublin University of Technology, Nadbystrzycka 40B, 20-618 Lublin, Poland; e.krawczak@pollub.pl
* Correspondence: s.gulkowski@pollub.pl; Tel.: +48-81-538-47-01

Abstract: The characterisation of photovoltaic modules requires a specialised laboratory that guarantees precise control of irradiance and its spectrum and control of the module temperature during testing. As an alternative, characteristic parameters can be extracted from the measurements of the current-voltage characteristics (*I-V* curves) carried out under outdoor conditions. This paper presents the results of the two commercial thin-film photovoltaic modules' characterisation. The first analysed device was a cadmium telluride (CdTe) photovoltaic module fabricated on glass, while the second was the flexible copper indium gallium diselenide (CIGS) PV module. The main parameters of the PV modules were extracted based on the series of *I-V* curve measurements under real operating conditions in Poland with the use of the capacitor-based *I-V* tracer. Solar radiation together with the modules' temperature were registered simultaneously with the *I-V* characterisation. Two approaches were proposed to estimate the main PV parameters at standard test conditions as output power, short circuit current or open circuit voltage. The difference in results of power for both approaches was below 1.5%. Energy, computed using the Osterwald model, was compared with the experimental measurements. The best results of absolute relative error (ARE) were found around 0.5% for both technologies. The lowest value of root mean squared error (RMSE) was 1.3% in terms of CdTe technology and 3.1% for CIGS.

Keywords: photovoltaic system; thin-film photovoltaics; *I-V* characteristic measurements; outdoor performance; building integrated photovoltaics

check for updates

Citation: Gulkowski, S.; Krawczak, E. Thin-Film Photovoltaic Modules Characterisation Based on *I-V* Measurements Under Outdoor Conditions. *Energies* **2024**, *17*, 5853. https://doi.org/10.3390/en17235853

Academic Editor: Enrique Romero-Cadaval

Received: 29 October 2024
Revised: 18 November 2024
Accepted: 19 November 2024
Published: 22 November 2024

Copyright: © 2024 by the authors. Licensee MDPI, Basel, Switzerland. This article is an open access article distributed under the terms and conditions of the Creative Commons Attribution (CC BY) license (https://creativecommons.org/licenses/by/4.0/).

1. Introduction

The world's energy demand is still growing. It is driven by a variety of factors: population growth, industrial development, societal evolution and, as a result, increased energy consumption in everyday life, to name but a few. Despite the great deal of efforts to decarbonize and reduce greenhouse gas (GHG) emissions, fossil fuels still dominate the global energy mix [1]. Moreover, fossil fuel combustion even increased in 2023 [2], accounting for 80% of global energy demand. Therefore, there is a strong need to accelerate the energy transition process from non-renewable to renewable energy sources (RESs), such as solar, wind, hydroelectric or geothermal energy. Solar energy is recognised as a primary energy source, and with the advancements in technology to improve its efficiency and cost reduction, and thus increase the affordability of such systems, it is expected that the use of this type of energy will soon be greater than the use of coal [3]. Critically important in the context of combating climate change, these systems do not cause air pollution [4].

Photovoltaic (PV) systems, which convert sunlight directly into electricity, have been significantly improved in recent years, leading to remarkable advances in the efficiency of solar cells. There are three generations of solar cells. The first generation, based on the crystalline silicon, is the most widely used technology on the market. The first generation of solar cells, based on silicon solar modules, currently achieves an efficiency of 24.9% [5]. However, the conception of combining the Si heterojunction with interdigitated back

contact technology resulted in a photovoltaic conversion efficiency of 26.7% with an area of 79 cm^2 [6]. The second generation, known as thin-film technology, includes modules made of CIGS, CdTe or amorphous silicon (a-Si). It is characterized by lower efficiency than the first generation, e.g., CIGS—19.2%, and CdTe—19.9%. According to [7], there is a strong interest in thin-film technology as it has emerged with higher relevance in publications than any other solar technology in recent years. However, the development of the first and the second generation is mostly achieved by changing the interface or device architecture rather than the absorber [6]. The third generation, which includes emerging technologies, such as organic modules (OPVs), dye-sensitized solar cells (DSSCs) [8] or perovskite solar cells, most of which are not yet available on the market, obtains 19.2% by perovskite modules [5]. However, the use of photovoltaic (PV) systems, which convert sunlight directly into electricity, is highly dependent on geographical location due to varying climatic conditions [9,10], thus resulting in fluctuation in energy production. Temperature and solar irradiance are the main factors which strongly affect the performance of PV installation [11]. Increasing the temperature of the module also strongly determines the conversion efficiency [12]. Thus, attention should be paid to the temperature coefficients (TCs), which represent the variation in working parameters as a function of temperature. As it has been shown in our previous works, understanding the relationship between outdoor environmental conditions and the operation of photovoltaic systems becomes a matter of great importance [13,14]. Hence, conducting the measurements in outdoor conditions, which deviates from standard test conditions (STC; T = 25 °C, G = 1000 W/m^2, AM = 1.5), is crucial [15].

For all these reasons, many researchers have examined the influence of outdoor conditions on the working parameters of photovoltaic modules. In the work of Kusznier and Wojtkowski [16], the influence of climatic conditions on the operation of PV systems was studied. The hybrid power plant located in Bialystok, Poland, consists of four photovoltaic sections, all made of the same PV modules, and two wind sections. The photovoltaic sets are installed on the roof and on the façade of the building. The research emphasizes that the efficiency of the PV installation is highly dependent on weather conditions, which fluctuate dynamically over time, with visible differences between the seasons. They indicated that the Global Horizontal Irradiation (GHI) can cause a ±20% shift in energy production, while the outdoor temperature can cause a ±10% shift in the efficiency.

Cañete et al. [17] analysed the performance of pc-Si modules, and different types of thin-film technology modules: amorphous silicon (a-Si), CdTe and tandem structure silicon (a-Si/μc-Si) under outdoor conditions. The measurements were carried out in Málaga, Spain. Due to temperatures exceeding 25 °C (STC), the registered daily efficiencies were lower than under STC, with losses ranging from 5% to 7.6%. The CdTe module had an efficiency loss of 5.4%. Researchers have shown that second-generation modules are more affected by high irradiation than modules of the first generation. The influence of outdoor parameters, such as irradiance and temperature, on the electrical output and efficiency of PV modules, was the subject of the investigation of Visa et al. [18]. The research was conducted over a period of 14 months in Brașov, Romania, which represents a temperate mountain climate. The working parameters of mono-, poly-crystalline silicon, CdTe, CIS and CIGS modules were examined. The findings indicate that the factor which influenced the most the photovoltaic conversion is solar radiation, and its components, namely direct and diffuse irradiance. Silicon-based modules exhibit superior performance stability compared to second-generation modules. They demonstrate relatively good performance and small efficiency losses, up to 10%, over the analysed period. Thin-film technology is more sensitive to changes in irradiance. Furthermore, higher temperatures result in higher efficiency losses. The group of Gasparin et al. [11] studied the changes in temperature coefficients as a function of irradiance. They determined the values of TCs on the basis of *I-V* characteristics measured at different temperatures. Their research concerned crystalline silicon modules: conventional and half-cut. Their findings indicate that the P_M (maximum power point) does not change significantly in the measurement range of

100–1000 W/m^2. However, silicon modules are more sensitive to temperature shifts at lower irradiance levels. Mehdi et al. [19] evaluated the influence of the temperature on the operating parameters, specifically the efficiency and performance ratio, of first-and second-generation modules, namely polycrystalline and cadmium telluride, in desert locations (Benguerir, Morocco). The measurements were carried out from May to October and showed that the PCE decreased by 8.7% and 6.8% for the polycrystalline silicon and CdTe modules, respectively, while the conversion efficiency decreased by 1.35% and 1.05% as the temperature shifted from 25 °C to 40°C. The work presented by Xu et al. [20] investigated the performance characteristics of flexible solar cells, such as silicon (Si), copper indium gallium selenide (CIGS) and perovskite, under different light irradiances. The PCE of the Si modules increased linearly with the increasing irradiance up to 1000 W/m^2, and then decreased. Analysis of how temperature affects the operation of a-Si and CIS modules is presented in the work of Perraki and Tsolkas [21]. The research was carried out in Patras (Greece), which represents a Mediterranean climate with an average irradiance of 4.2 kWh/d and an average outdoor temperature of 17.7 °C. The findings indicate that the short-circuit current is slightly affected by temperature shifts, with an increasing *Isc* value as the temperature increases. The correlation with the V_{OC} value is far stronger. In both cases, open-circuit voltage declines with the increasing temperature. However, the greater reduction was observed for the CIS module. The overall efficiency of CIS modules dropped significantly when the temperature exceeded 100 °C, while the PCE of the a-Si modules remained the same.

This work fits in with the studies on photovoltaic characterization of the module based on the current-voltage measurements under real outdoor operation conditions. To the best of our knowledge, there are insufficient works related to thin-film PV modules characterisation carried out in the high-latitude locations such as Poland. The proposed methods of characterisation allow for the easy and convenient estimation of the PV modules' actual power, and thus the efficiency at location of the PV system without moving the PV modules or using expensive indoor equipment. Two converging approaches were proposed. Moreover, the comparison of the PV module temperature with the temperature of a monocrystalline silicon reference cell was shown.

2. Materials and Methods

2.1. Experimental Setup

The experimental system (Figure 1) consisted of photovoltaic (PV) modules, the reference cell, the Pt100 surface temperature sensor (PV-Engineering GmbH, Iserlohn, Germany) and the *I-V* measurement device which was placed on the terrace of the building located in Poland (latitude of 51°13′ N, longitude of 22°29′ E). The location ensured the natural ventilation of the PV modules under scrutiny. Two thin-film technologies were taken into consideration. The first one is based on a cadmium telluride absorber (CdTe) and the second one is based on copper indium gallium diselenide (CIGS). Both PV modules were installed on a horizontal plane. The reference cell was attached to the PV module or in its vicinity to measure the irradiance in the plane of the PV modules. Before the measurements, the PV modules and the reference cell were cleaned thoroughly to avoid the impact of soiling on the results. The temperature surface sensor Pt100 was attached to the back side of the PV module to measure its temperature. Additionally, the temperature of the reference cell was registered using the Pt1000 sensor (PV-Engineering GmbH, Iserlohn, Germany) for comparative analysis.

The detailed specification of the PV modules provided by the manufacturer is presented in Table 1, while the specification of the reference cell is given in Table 2. The tested PV modules were part of the PV system working for a couple of years.

The back surface temperature was measured using the RTD surface sensor Pt100. The device allows for measurements in the range between −30 °C and +105 °C with uncertainty of ±(0.15 °C + 0.002·T). The uncertainty of the reference cell with incident

radiation perpendicular to the surface of the PV module and AM = 1.5 was ±2% (±7 W/m^2). In general, this value is not higher than ±5%.

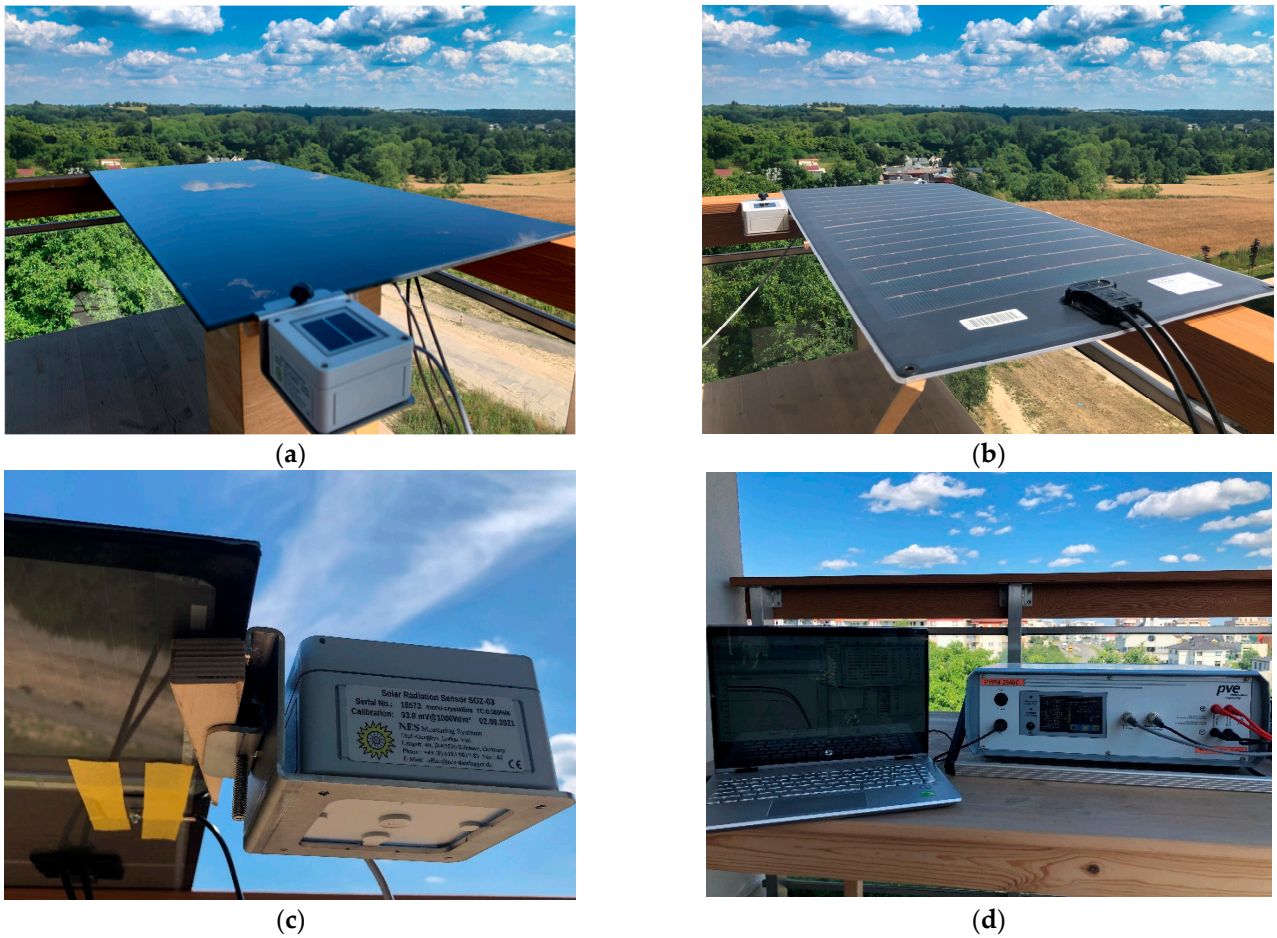

Figure 1. The experimental setup: (**a**) PV module of CdTe technology; (**b**) PV module of CIGS technology; (**c**) the reference cell and temperature surface sensor; (**d**) the *I-V* measurement device.

Table 1. Electrical parameters of the PV modules under study.

PV Module Characteristics	CdTe	CIGS
Maximum power under STC $P_{m,ref}$ (Wp)	75 (+/−5%)	55.0
Open-circuit voltage $V_{oc,ref}$ (V)	62.0	21.0
Nominal voltage $V_{mpp,ref}$ (V)	46.3	17.0
Short-circuit current $I_{sc,ref}$ (A)	1.95	3.7
Nominal current $I_{mpp,ref}$ (A)	1.65	3.2
Efficiency (%)	10.6	14
Temperature coefficient of V_{oc} (%/°C)	−0.24	−0.28
Temperature coefficient of I_{sc} (%/°C)	0.02	0.008
Temperature coefficient of power (%/°C)	−0.25	−0.38
PV panel area (m^2)	0.72	0.39

The current-voltage (*I-V*) characterisation of the PV modules under outdoor operating conditions (OPC) was carried out using the PVPM 2540C *I-V* tracer (PV-Engineering GmbH, Iserlohn, Germany), which measured the *I-V* curves at a capacitive load. The undoubted advantage of the applied measurement method was its fast sweep speed. It allowed for the collection of the whole *I-V* curve within a short time period, which is crucial to obtain all measurands in the same weather conditions, mainly the irradiance and the temperature of the PV module [22]. Moreover, the applied device allows for the

synchronous collection of the *I-V* curves with the irradiance and the temperature of the module. The device is characterized by a high *I-V* characteristic measurement accuracy. The most relevant parameters, including the measurement precision of the *I-V* tracer, are shown in Table 3. Both the reference cell and the temperature sensors were parts of the PVPM 2540C measurement system calibrated by the manufacturer. The calibration factor of the reference cell is shown in Table 2.

Table 2. The specification of the reference cell.

Reference Cell Characteristics	SOZ-03
Cell technology	mono-crystalline silicon
Radiation range (W/m^2)	100–1200
Calibration coefficient ($mV/kW/m^2$)	93.8
Uncertainty (%)	±2 (<5%)
Temperature coefficient (%/°C)	0.06
Size of the cell (cm^2)	5 × 5

Table 3. The specification of the PVPM2540C *I-V* tracer.

I-V Tracer Characteristics	PVPM 2540C
Sweep speed (s)	0.02–2.0
Voltage measurement range (V)	25–250
Current measurement range (A)	2–40
Voltage resolution (V)	0.01–0.25
Current resolution (A)	0.005–0.01
I-V curve measurement uncertainty (%)	±1.0
Peak power measurement uncertainty (%)	±5.0
Operating temperature conditions (°C)	0–50

2.2. Methods of Data Processing and Analysis

The *I-V* curve measurements were carried out during sunny weather conditions around the solar noon to minimize the impact of irradiance and temperature fluctuation on the results. A total of 255 *I-V* curves were recorded, of which 221 (87%) were removed after the filtering process. Common data quality check procedures for performance evaluation were applied to ensure the accuracy of computations. Data measured under irradiance lower than 700 W/m^2 were excluded. High cutoff was set at 1200 W/m^2. The computations were performed using Matlab/Simulink software R2023a [23] (Mathworks, Natick, MA, USA).

The *I-V* characteristics were drawn and visually checked to confirm their suitable shape. Incomplete and bad-shaped curves were removed from the dataset. Following the recommendation of [24], only the curves measured under the irradiance higher than 700 W/m^2 were taken into account. Moreover, the curves measured under wind speed higher than 2 m/s were discarded.

A single *I-V* curve was composed of 101 current-voltage (I,V) discrete points. For each *I-V* curve, parameters such as short circuit current (I_{sc}), open circuit voltage (V_{oc}), maximum current (I_m), maximum voltage (V_m) and maximum power (P_m) were found using the methods described in [25–27]. The maximum power was computed based on the power–voltage (*P-V*) curve, for which the greatest value P_z was found. Then, all the experimental points P_i near the P_z, which satisfied the condition $P_i \geq 0.85\ P_z$, were modelled using a fourth-order polynomial fit. Maximum power (P_m) was determined from the first derivative of the fit. The short circuit current (0, I_{sc}) of the *I-V* curve and the open circuit voltage (V_{oc}, 0) were computed by applying the linear fits close to both points. Due to the data quality check procedure, a one-dimensional threshold was set to select the *I-V* points for the fitting in each case. In terms of I_{sc}, all the experimental points (I,V) which fell within the range of voltage (0–20% of $V_{oc,ref}$) were taken into consideration, whereas for the computation of V_{oc} all the points within the range of current (0–20% of $I_{sc,ref}$) were

included. The intersections of linear fits with axes made it possible to find the exact values of short circuit current and open circuit voltage. Moreover, based on the slope (dI/dV), experimental series resistance (R_s) of the PV module could be determined according to Equation (1).

$$R_S = -\left(\frac{dV}{dI}\right)_{V=V_{oc}} \quad (1)$$

Figure 2 shows the notable points extracted using the above-described method. All the points were marked with squares. Moreover, the solid line shows the results of the linear fit applied to the *I-V* curve for short circuit current and open circuit voltage computation. Results of polynomial fit were also marked by the line on the *P-V* plot. The presented curve was measured under G = 905.5 W/m^2. The temperature of the PV module was 49.7 °C. Maximum power point computed using the applied method was P_m = 54.269 W, while the value of 54.235 W was found based only on the measured points. The series resistance was equal to 5.77 Ω. The rest of the characteristic points' values were as follows: V_{oc} = 50.4 V, I_{sc} = 1.77 A. Such procedure was applied to all the curves under scrutiny.

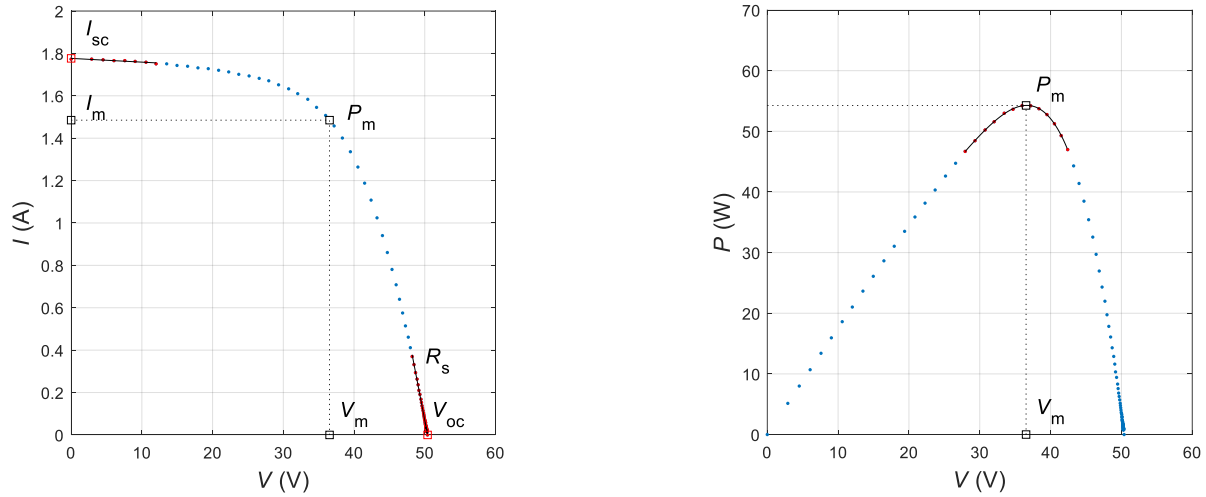

Figure 2. One of the measured (**a**) *I-V* curve and (**b**) *P-V* curve of CdTe PV module. The characteristic points as well as linear and fourth-order polynomial fits were marked using squares and lines, respectively.

In order to obtain the characteristic parameters of the tested PV modules at the reference conditions, two different approaches were applied and the final results were compared. In the first method, all the measured curves that satisfied the filter conditions were translated from real operating to the standard test conditions according to the IEC 60891:2021 [28] and the methods described in the work of [29] with the use of Matlab's functions provided in the PVLIB library [30]. The current and voltage of a single *I-V* curve was transferred to STC using Equations (2) and (3), respectively.

$$I_{i,STC} = I_i + I_{i,sc}\cdot\left(\frac{1000\ \text{W/m}^2}{G_i} - 1\right) + \alpha_{Isc}\cdot(25\ ^\circ\text{C} - T_i), \quad (2)$$

$$V_{i,STC} = V_i - R_s(I_{i,STC} - I_i) - \kappa\cdot I_{i,STC}\cdot(25\ ^\circ\text{C} - T_i) + \beta_{Voc}\cdot(25\ ^\circ\text{C} - T_i), \quad (3)$$

where

$I_{i,STC}$—current after translation to standard test conditions, STC (in A);
$V_{i,STC}$—voltage after translation to STC (in V);
I_i—current at real operating conditions (OPC) before the translation to the STC (in A);
$I_{i,sc}$—short circuit current at OPC (in A);

G_i—irradiance measured during the *I-V* sweep at OPC (in W/m^2);
α_{Isc}—temperature coefficient of short circuit current at OPC (in A/°C);
β_{Voc}—temperature coefficient of open circuit voltage (in V/°C) at STC (provided by the manufacturer);
T_i—module temperature during the *I-V* measurement at OPC (°C);
R_s—series resistance of the PV module (Ω) at OPC;
κ—temperature coefficient of series resistance (Ω/°C).

Values of 1000 W/m^2 and 25 °C in Equations (2) and (3) stand for the reference irradiance and module temperature, respectively.

Following the work of [29,31], the dependency of the short circuit current temperature coefficient on irradiance is given by Equation (4).

$$\alpha_{Isc} = \alpha_{STC} \cdot \left(\frac{G_1}{1000\ \mathrm{W/m^2}} \right), \tag{4}$$

where α_{STC} is the temperature coefficient of short circuit current (in A/°C) at reference conditions (provided by the manufacturer).

Series resistance was computed using Equation (5).

$$R_s = R_{s,STC} + \kappa \cdot (T_1 - 25\ ^\circ\mathrm{C}) \tag{5}$$

where $R_{s,STC}$ is the series resistance of the PV module (Ω) at OPC.

Both series resistance values were estimated using the method presented in the work of [24], which was based on the linear regression of plotting the *Rs* values vs. temperature. $R_{s,STC}$ and κ were estimated from the equation of linear fit.

After the translation of the measured *I-V* curves to STC, the characteristic parameters, i.e., short circuit current, open circuit voltage, maximum current and voltage and maximum power were determined using the same procedure as described earlier. Median values of these parameters were considered as the final reference parameters (STC) of the PV modules. Further analysis related to energy estimation was carried out using maximum power point $P'_{m,STC}$ (W).

In the second approach, power at the reference conditions $P''_{m,STC}$ (W) was obtained using the linear regression fit applied to the relation given by Equation (6). This method was successfully used by several researchers, e.g., [27,32].

$$P_{i,t=25^\circ\mathrm{C}} = \frac{P''_{m,STC}}{1000\ \mathrm{W/m^2}} \cdot G_i \tag{6}$$

where

$P_{i,t=25^\circ\mathrm{C}}$—experimental output power corrected to the temperature of 25 °C (in W);
$P''_{m,STC}$—experimental peak power at standard test conditions (in W).

The temperature correction was made based on Equation (7).

$$P_{i,t=25^\circ\mathrm{C}} = \frac{P_i}{1 + \gamma(T_i - 25\ ^\circ\mathrm{C})} \tag{7}$$

where γ is the temperature coefficient of the power (in 1/°C) which was taken from the manufacturer's datasheet.

Following the recommendation stated in [33], data corresponding to the irradiance lower than 700 W/m^2 were not included. Linear fit of the relation given by Equation 6 was forced to cross the (0,0) point using the function polyfitZero provided in Matlab by [34].

In order to compare the two methods of determining the maximum power point, the result of the energy production simulation was compared with its real (experimental) value. For the simulation, the obtained reference maximum power points, $P'_{m,STC}$ and $P''_{m,STC}$, were used following the method presented in the previous work [35].

The energy E_i of i-th power output $P_{m,i}$ at time interval τ (in min) was computed using Equation (8) [36].

$$E_i = P_i \cdot \tau \tag{8}$$

where τ = 1 min. The total electricity E_{tot} generated during the measurement period was given by Equation (9).

$$E_{tot} = \sum_{i=1}^{N} E_i \tag{9}$$

where N determines the total number of experimental points.

The absolute relative error (ARE, in %) of the energy was computed using Equation (10) [37], while root mean square error (RMSE) was obtained from Equation (11) [38].

$$ARE(\%) = \frac{\left| E_{tot,computed} - E_{tot,measured} \right|}{E_{tot,measured}} \cdot 100\% \tag{10}$$

$E_{tot,computed}$ and $E_{tot,measured}$ were the simulated and experimental total electricity produced by the PV module, respectively.

$$RMSE(\%) = 100 \cdot \frac{\sqrt{N \sum \left(P_{computed} - P_{measured} \right)^2}}{\sum P_{measured}}, \tag{11}$$

where N is the number of measured power points.

Figure A1 (Appendix A) shows the flowchart of the methods applied in the work.

3. Results and Discussion

Figure 3 shows the dependency of the short circuit current on in-plane irradiance. Each point corresponds to the I_{sc} value of the measured *I-V* curve. The linear trend can be clearly visible in both technology modules PV under scrutiny. The correlation coefficient R^2 related to the results of CdTe was found to be 0.96, while for CIGS it was equalled to 0.84. The RMSE was found to be of 0.6% and 1.3% for CdTe and CIGS, respectively. Based on the linear regression equation fitted to the data, the reference value of short circuit current was 1.96 A in terms of CdTe (see Figure 3a) and 3.59 A for CIGS (Figure 3b). It should be mentioned that the computed reference values did not include the temperature influence on I_{sc}. However, due to the low-temperature coefficients of the current, this influence can be neglected.

The dependency of the open circuit voltage on the PV modules' temperature is shown in Figure 4. According to the negative temperature coefficient of voltage presented in Table 1, open circuit voltage was decreasing with the temperature. Clearly, a linear trend could be visible for both PV modules under study. The correlation coefficients of linear fit were slightly below 0.9. The RMSE was about 0.6% in terms of CIGS, while for CdTe it was found to be of 1%. Neglecting the second-order effect related to the influence of the irradiance on the V_{oc} the reference values of the open circuit voltage were estimated as 52.8 V and 19.8 V in terms of CdTe and CIGS, respectively.

As it was previously mentioned, the temperature of the reference cell was measured using a Pt1000 sensor installed inside the device. The PV module temperature was measured using the Pt100 sensor attached to the back side of the PV module. The results of both measurements under the irradiance over 700 W/m^2 are shown in Figure 5. The measurements were conducted on various sunny days. That is why the temperature of the reference cell is different in both figures. However, in the whole range of irradiances, CdTe technology revealed a lower module temperature than the reference cell. The mean value differed by about 5 °C, while the mean temperature of the CIGS module was found to be higher by about 10 °C than the temperature of the reference cell. The maximum registered value of the temperature of the CdTe module was about 55 °C, while the reference

cell's maximum temperature equalled 59.0 °C. In terms of CIGS, the maximum module temperature was 65 °C, while the reference cell recorded the maximum temperature of 53 °C. Such differences revealed that the various technologies as well as the encapsulation of PV modules could have a significant impact on their temperature at high irradiances.

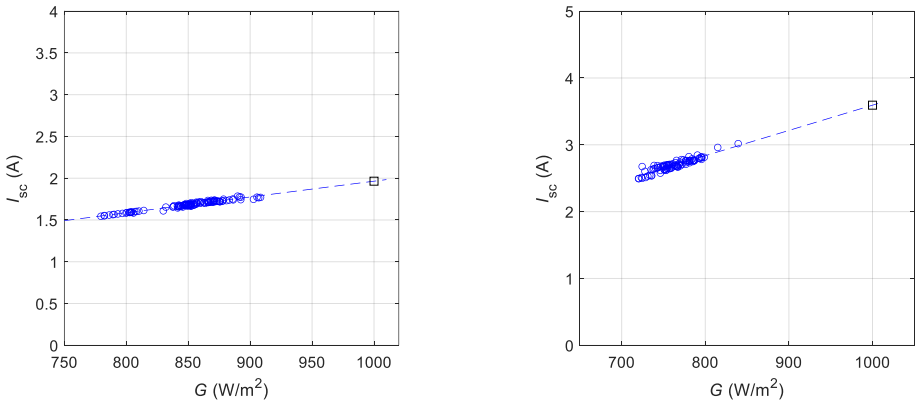

Figure 3. Short circuit current dependency on the in-plane irradiance: (**a**) CdTe and (**b**) CIGS. The reference values at 1000 W/m^2 were marked by the square.

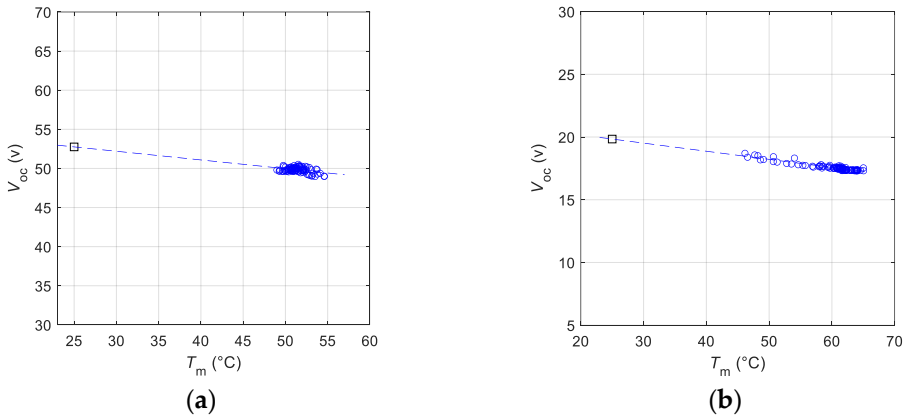

Figure 4. Open circuit voltage dependency on the temperature of the PV module: (**a**) CdTe and (**b**) CIGS. The reference values at 25 °C were marked by the square.

Figure 6 shows the dependency of the DC output power on in-plane irradiance. Obviously, with the increasing irradiance power, the output of both PV modules was also increased with the linear trend. Figure 6 also shows the dependency of the power output on the temperature of the PV module, which is higher at high irradiance, than the reference temperature of 25 °C. Because of this dependency, all the experimental points were firstly transferred to the reference temperature (25 °C), according to Equation (7), and then the linear fit was applied (Equation (6)). It should be emphasized that the linear fit was forced to cross the (0,0) point. Based on the equations of the linear fit (shown in Figure 6), the experimental power at reference conditions was estimated ($P''_{m,STC}$). In terms of the CdTe technology PV module, the value of 64.4 W was obtained, while for CIGS the power was 43.5 W. The correlation coefficients were 0.90 and 0.65 for CdTe and CIGS, respectively. The RMSE was found to be 1.1% for CdTe and 2.0% in terms of CIGS. The above-discussed method showed easy and fast estimation of the reference parameters of the PV module by measuring parameters such as DC output power, short circuit current, and open circuit voltage together with the irradiance and module temperature.

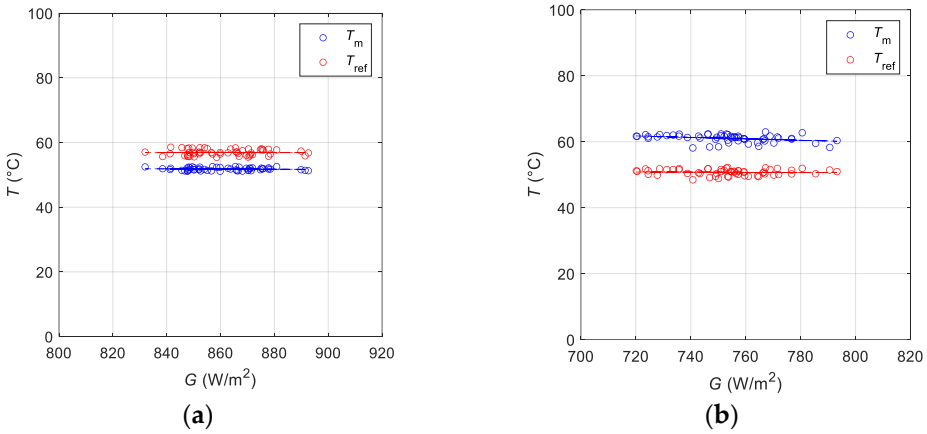

Figure 5. Comparison of the temperature of the reference cell used for irradiance measurements and the temperature of the PV module: (**a**) CdTe and (**b**) CIGS.

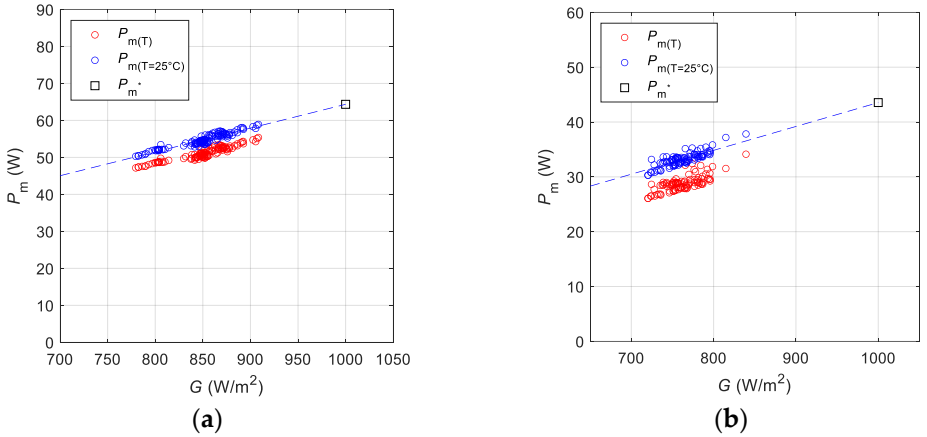

Figure 6. The dependency of the output power on in-plane irradiance after the correction of the temperature to the reference value of 25 °C. The experimental reference output power at 1000 W/m^2 was marked by the square: (**a**) CdTe and (**b**) CIGS.

The second approach of obtaining the reference parameters estimation together with voltage and current at maximum power point was based on the translation the experimental *I-V* curves to standard test conditions using Equations (2) and (3). Figures 7 and 8 show the *I-V* characteristics before and after the translation. As shown in the figures, the translated curves in both studied thin-film technologies revealed a narrower distribution. Due to the measurement under irradiance being below 1000 W/m^2 and the temperature of the module being above 25 °C, the procedure of linear fittings in the vicinity of open circuit voltage and short circuit points described in the previous section was applied.

The median values of the short circuit current extracted from the curves after the translation to standard test conditions (STC) were 1.97 A and 3.53 A for CdTe and CIGS, respectively. As can be seen, the values of I_{sc} are very close to those obtained by the previous method (compared with 1.96 A and 3.59 A for CdTe and CIGS, respectively). The interquartile range of I_{sc} for CIGS was found from 2.49 A to 2.85 A (0.36 A) at operating conditions, while after the transformation to the standard test it was found between 3.49 A and 3.57 A (0.08 A). In terms of CdTe technology, the spread of the data is even lower. The interquartile range was found to be between 1.66 A and 1.72 A (0.06 A) at OPC and from 1.96 A to 1.97 A (0.01 A) at STC. Both values proved the high precision of the short circuit current estimation.

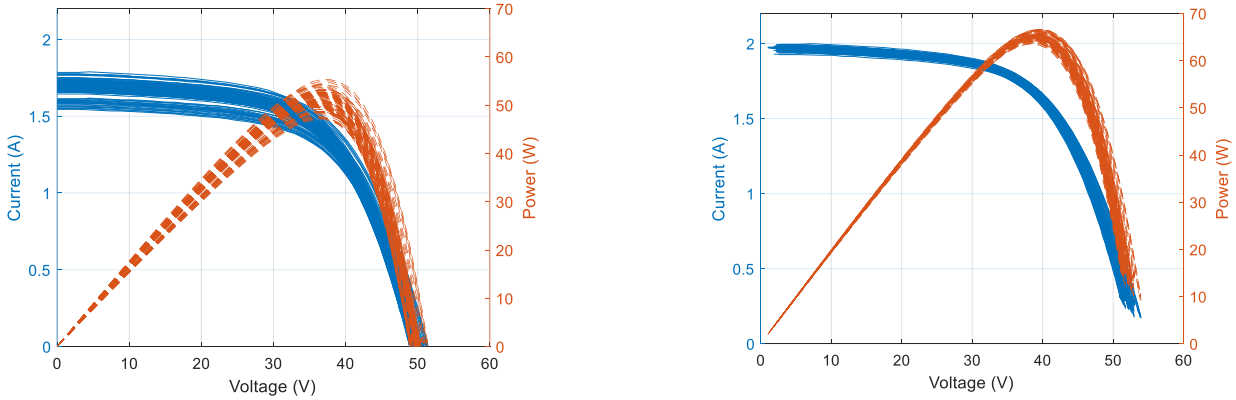

Figure 7. Series of the *I-V* and *P-V* curves of CdTe technology PV module: (**a**) measured at operational conditions (OPC) and (**b**) transferred to reference conditions (STC).

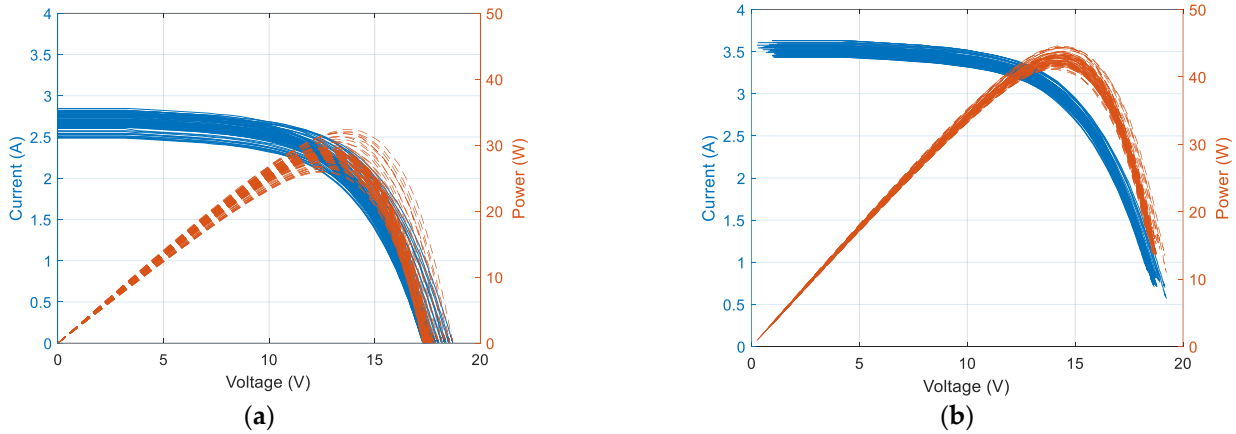

Figure 8. Series of the *I-V* and *P-V* curves of CIGS technology PV module: (**a**) measured at operational conditions (OPC) and (**b**) transferred to reference conditions (STC).

A similar low spread range of the open circuit voltage values was found for CIGS technology. The interquartile range changed from 0.26 V at OPC to 0.07 V at STC in which the 25th quartile was found as 19.68 V while the 75th was equal to 19.75 V. The median value of V_{oc} after the translation process was 19.71 V (CIGS). Regarding the CdTe technology, the estimated V_{oc} was found as 53.6 V with an interquartile range between 53.3 V and 54.1 V.

The median values of the maximum power point at the STC were 42.9 W and 65.1 W for CIGS and CdTe, respectively. In both cases, the obtained values were very close to those obtained by the previous method. The difference was found below 1.4% in terms of CIGS technology and 1% for CdTe. This proved that both methods lead to precise estimation of the PV module power. The interquartile range after translation to STC was found between 41.4 W and 43.48 W in terms of CIGS and from 64.6 W to 65.5 W in terms of CdTe. The median values of voltage at maximum power point (STC) were 39.0 V (CdTe) and 14.2 V (CIGS), while the median values of the current were 1.67 A and 2.99 A for CdTe and CIGS, respectively. Figure 9 shows normalised (to datasheet values) characteristic parameters of the PV modules under scrutiny before (at OPC) and after the translation (at STC). As can be noticed, the estimated values of maximum power points were found to be lower than those provided by the manufacturer in the datasheet (Table 1). It should be emphasised that the investigated modules were not new. The reduction in output power might be caused by the degradation effects that take place during the operation of the PV modules in the PV systems.

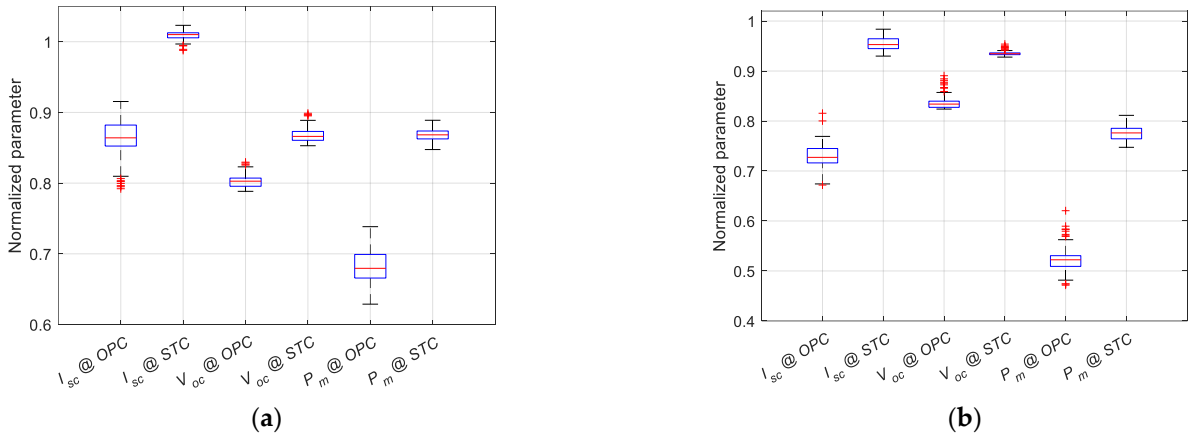

Figure 9. Normalised characteristic parameters of the PV modules: (**a**) CdTe and (**b**) CIGS.

Based on the output power estimated by both presented methods, the energy was computed using the Osterwald model [39] according to the approach presented in previous papers [35]. Figure 10 shows the comparison of the computation results with the experimental measurements during the sunny days in the period of the day with the highest irradiance values.

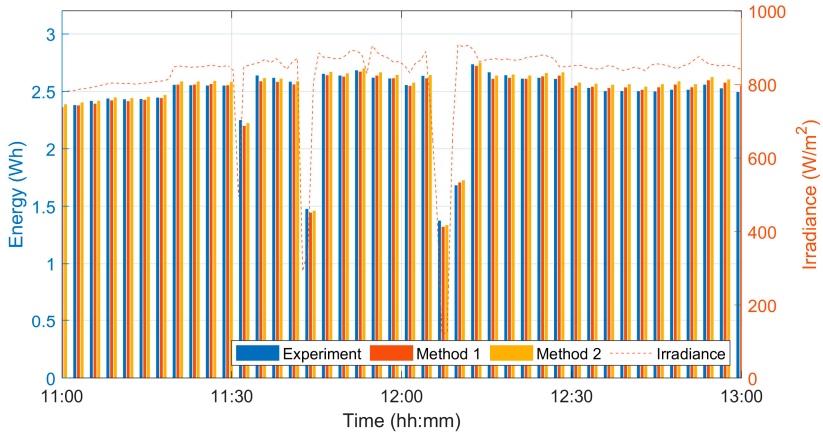

Figure 10. Comparison of the experimental energy and energy computed with estimated power by both methods during the sunny day for (**a**) CdTe and (**b**) CIGS module.

Regarding the CdTe technology, energy computed with the power obtained by the first method (based on experimental power points) was almost equal to the experimental

energy measured during the presented period. The absolute relative error was lower than 0.5%. In terms of the second approach, related to the conversion of the *I-V* curves, the relative error was found to be higher (1.1%). The RMSE values were 1.3% and 1.7% for the first and second methods, respectively. The relative error of CIGS technology in both methods was found to be below 1%, showing the better accuracy of the first method of the power estimation with a relative error of 0.5%. The RMSE was also slightly better in the case of the first method (3.1%), while for the second it was 3.5%.

Similarly to our findings, the linear dependency of open circuit voltage on the temperature of the PV module for CdTe technology was shown in the work of [40]. The higher range of temperatures was achieved by the external cooling system of the PV modules. It should be mentioned that, with the use of a capacitor-based *I-V* analyser, the difference between indoor and outdoor measurements was around 1%. The *I-V* tracer capacitor was also used for the experimental setup system for organic PV modules' characterisation by [41] and in our previous work on heterojunction with an intrinsic thin-layer photovoltaic module [42]. The same technology of measuring device was used in this research. Numerous solutions of the data acquisition systems were reviewed in the work of [43], which proves the importance of the PV system characterisation. The flexible CIGS PV module as well as CdTe technology were also investigated by [12]. Similarly to our work, the authors observed the module temperature of CdTe technology in the range between 54 °C and 57 °C (55 °C in this work) at high irradiances for locations up to 1000 m above the sea level. In terms of CIGS, a slightly lower maximum temperature than in our case was observed (61.2 °C); however, this technology also reached the highest value of average temperature among all the investigated technologies (cadmium telluride, organic photovoltaic or the amorphous one). The authors presented a measurement error below 1% for the tested parameters during high irradiances. This is in accordance with the recommendation, and it is also applied in this work to keep the irradiance at a high level during the performance assessment.

4. Conclusions

The results of the main parameters of the PV modules' estimation under standard test conditions of the two commercial thin-film photovoltaic modules were shown. CdTe fabricated on glass together with flexible CIGS technology was investigated. The *I-V* characterisation was carried out under real outdoor operating conditions in Poland with the use of the capacitor-based *I-V* tracer together with the reference cell and Pt100 surface sensor for irradiance and module temperature measurements, respectively. The results of two approaches, which gave very similar results of characteristic parameters under standard test conditions, were shown. With the first approach, the output power, short circuit current and open circuit voltage were estimated in a fast and easy way, while usage of the second method required more advanced computations. However, this method led to obtaining the whole *I-V* curves at standard test conditions based on which any parameter of interest could be found, e.g., current and voltage at the maximum power point. From a practical point of view, both approaches allowed for the estimation of PV modules' parameters in the location of the PV system. There was no need to transport the PV modules.

Absolute relative error (ARE) with root mean squared error (RMSE) were used to compare the obtained results of power and energy (by the Osterwald method) with the experimental measurements. In terms of the CdTe technology, the power obtained by both methods was 64.4 W and 65.1 W with RMSE values of 1.3% and 1.7%, respectively. The absolute relative error values of energy were 0.5% and 1.1%. For CIGS, the estimated power was 43.5 W using the first method, while for the second it was 42.9 W. The RMSE values were 3.1% and 3.5%, respectively. The ARE values of energy were 0.5% and slightly below 1%. A significant difference was noted when comparing the reference cell temperature with the measured temperature of the PV module by the Pt100 sensor. Regarding the CdTe technology fabricated on glass, the temperature of the module was lower at high irradiance

with a difference of about 5 °C, while the temperature of the CIGS flexible module was higher by about 10 °C than the temperature of the reference cell.

Future work will include the usage of a good-quality pyranometer for irradiance measurements and the weather station for outdoor conditions monitoring. Long-term campaign would make it possible to collect more data measured under various weather conditions. The usage of calibrated or new PV modules would make it possible to estimate the precision of the presented characterisation approaches.

Author Contributions: Conceptualisation, S.G.; methodology, S.G. and E.K.; software, S.G. and E.K.; validation, S.G.; formal analysis, S.G.; investigation, S.G. and E.K.; data curation, S.G. and E.K.; writing—original draft preparation, S.G. and E.K.; visualisation, S.G. and E.K.; supervision, S.G. All authors have read and agreed to the published version of the manuscript.

Funding: This research was funded by Faculty of Environmental Engineering, Lublin University of Technology, Poland, grant number FD-20/IS-6/013 and FD-20/IS-6/018.

Data Availability Statement: Data are contained within the article.

Acknowledgments: Authors would like to thank José Vicente Muñoz Diez from University of Jaén, Spain for recommendation of measurement device.

Conflicts of Interest: The authors declare no conflicts of interest.

Appendix A

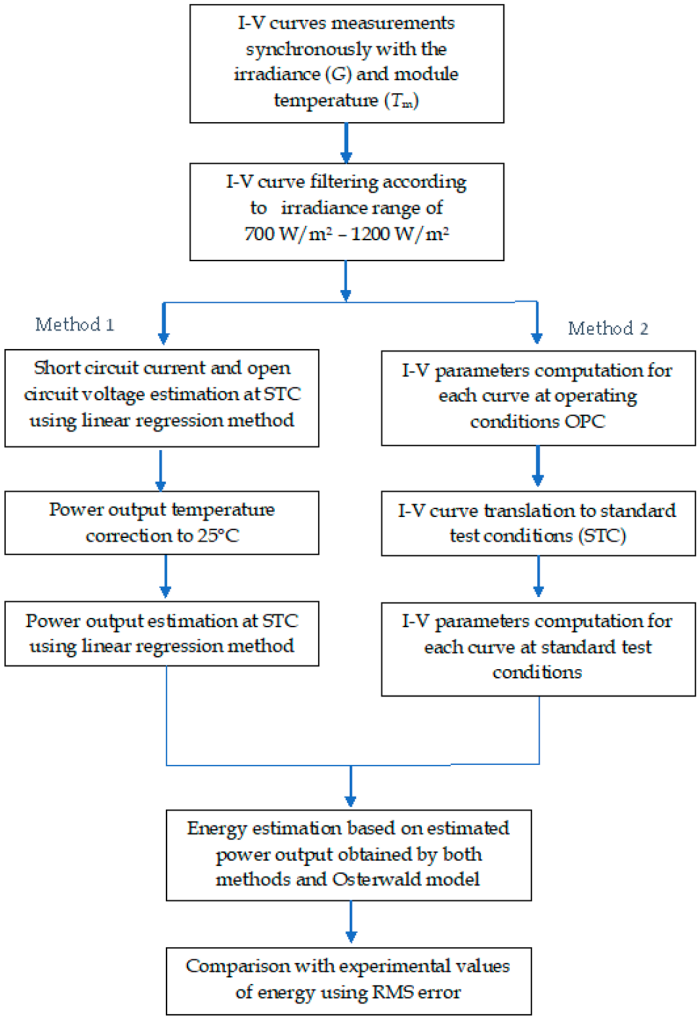

Figure A1. Flowchart of the applied methods.

References

1. IEA. *World Energy Outlook 2023*; International Energy Agency (IEA): Paris, France, 2024.
2. Davenport, J.; Wayth, N. *Statistical Review of World Energy*, 73rd ed.; Energy Institute: London, UK, 2024.
3. IEA. *Renewables 2022. Analysis and Forecast to 2027*; International Energy Agency (IEA): Paris, France, 2023; p. 159.
4. Hysa, B.; Mularczyk, A. PESTEL Analysis of the Photovoltaic Market in Poland—A Systematic Review of Opportunities and Threats. *Resources* **2024**, *13*, 136. [CrossRef]
5. Philipps, D.S.; Ise, F.; Warmuth, W.; GmbH, P.P. *Photovoltaics Report 2024*; Fraunhofer ISE: Freiburg, Germany, 2024.
6. Nayak, P.K.; Mahesh, S.; Snaith, H.J.; Cahen, D. Photovoltaic solar cell technologies: Analysing the state of the art. *Nat. Rev. Mater.* **2019**, *4*, 269–285. [CrossRef]
7. Reyes-Belmonte, M.A. Quo Vadis Solar Energy Research? *Appl. Sci.* **2021**, *11*, 3015. [CrossRef]
8. Krawczak, E.; Zdyb, A. The Effect of Electrode Immersion Time and Ageing on N719 Dye-Sensitized Solar Cells Performance. *J. Ecol. Eng.* **2020**, *21*, 53–60. [CrossRef]
9. Ollas, P.; Thiringer, T.; Chen, H.; Markusson, C. Increased photovoltaic utilisation from direct current distribution: Quantification of geographical location impact. *Prog. Photovolt. Res. Appl.* **2021**, *29*, 846–856. [CrossRef]
10. Saglam, S. Meteorological Parameters Effects on Solar Energy Power Generation. *WSEAS Trans. Circuits Syst.* **2010**, *9*, 637–649.
11. Perin Gasparin, F.; Detzel Kipper, F.; Schuck de Oliveira, F.; Krenzinger, A. Assessment on the variation of temperature coefficients of photovoltaic modules with solar irradiance. *Sol. Energy* **2022**, *244*, 126–133. [CrossRef]
12. Martínez-Deusa, S.J.; Gómez-García, C.A.; Velasco-Medina, J. A Platform for Outdoor Real-Time Characterization of Photovoltaic Technologies. *Energies* **2023**, *16*, 2907. [CrossRef]
13. Gulkowski, S.; Krawczak, E. Long-Term Energy Yield Analysis of the Rooftop PV System in Climate Conditions of Poland. *Sustainability* **2024**, *16*, 3348. [CrossRef]
14. Krawczak, E. A Comparative Analysis of Measured and Simulated Data of PV Rooftop Installations Located in Poland. *Energies* **2023**, *16*, 5975. [CrossRef]
15. Elibol, E.; Özmen, Ö.T.; Tutkun, N.; Köysal, O. Outdoor performance analysis of different PV panel types. *Renew. Sustain. Energy Rev.* **2017**, *67*, 651–661. [CrossRef]
16. Kusznier, J.; Wojtkowski, W. Impact of climatic conditions on PV panels operation in a photovoltaic power plant. In Proceedings of the 2019 15th Selected Issues of Electrical Engineering and Electronics (WZEE), Zakopane, Poland, 8–10 December 2019; pp. 1–6.
17. Cañete, C.; Carretero, J.; Sidrach-de-Cardona, M. Energy performance of different photovoltaic module technologies under outdoor conditions. *Energy* **2014**, *65*, 295–302. [CrossRef]
18. Visa, I.; Burduhos, B.; Neagoe, M.; Moldovan, M.; Duta, A. Comparative analysis of the infield response of five types of photovoltaic modules. *Renew. Energy* **2016**, *95*, 178–190. [CrossRef]
19. Mehdi, M.; Ammari, N.; Merrouni, A.A.; Dahmani, M.; Benazzouz, A. Outdoor Experimental Investigation of the Temperature Effect on the Performance of Different PV Modules Materials. *Key Eng. Mater.* **2023**, *954*, 111–121. [CrossRef]
20. Xu, W.; Wang, C.; Lu, C.; Sun, H.; Wang, X.; Sun, Y.; Lv, L. Weak Light Characteristic Acquisition and Analysis of Thin-Film Solar Cells. In *Proceedings of the Communications, Signal Processing, and Systems*; Liang, Q., Wang, W., Liu, X., Na, Z., Li, X., Zhang, B., Eds.; Springer: Singapore, 2021; pp. 1448–1456.
21. Perraki, V.; Tsolkas, G. Temperature Dependence on the Photovoltaic Properties of Selected Thin-Film Modules. *Int. J. Sustain. Green Energy* **2013**, *2*, 140–146. [CrossRef]
22. Zhu, Y.; Xiao, W. A comprehensive review of topologies for photovoltaic I–V curve tracer. *Sol. Energy* **2020**, *196*, 346–357. [CrossRef]
23. The MathWorks Inc. *MATLAB Version: 9.14.0 (R2023a)*; The MathWorks Inc.: Natick, MA, USA, 2023. Available online: https://www.mathworks.com/ (accessed on 30 September 2024).
24. Piliougine, M.; Spagnuolo, G.; Sidrach-de-Cardona, M. Series resistance temperature sensitivity in degraded mono–crystalline silicon modules. *Renew. Energy* **2020**, *162*, 677–684. [CrossRef]
25. Smith, R.M.; Jordan, D.C.; Kurtz, S.R. *Outdoor PV Module Degradation of Current-Voltage Parameters*; NREL: Denver, CO, USA, 2012; pp. 2547–2554.
26. Piliougine, M.; Guejia-Burbano, R.A.; Petrone, G.; Sánchez-Pacheco, F.J.; Mora-López, L.; Sidrach-de-Cardona, M. Parameters extraction of single diode model for degraded photovoltaic modules. *Renew. Energy* **2021**, *164*, 674–686. [CrossRef]
27. Montes-Romero, J.; Almonacid, F.; Theristis, M.; de la Casa, J.; Georghiou, G.E.; Fernández, E.F. Comparative analysis of parameter extraction techniques for the electrical characterization of multi-junction CPV and m-Si technologies. *Sol. Energy* **2018**, *160*, 275–288. [CrossRef]
28. IEC 60891:2021—Photovoltaic Devices—Procedures for Temperature and Irradiance Corrections to Measured I-V Characteristics. Available online: https://standards.iteh.ai/catalog/standards/iec/f3c311fd-1810-4281-bb6d-094c2df6e263/iec-60891-2021 (accessed on 28 October 2024).
29. Piliougine, M.; Sánchez-Friera, P.; Spagnuolo, G. Comparative of IEC 60891 and Other Procedures for Temperature and Irradiance Corrections to Measured I–V Characteristics of Photovoltaic Devices. *Energies* **2024**, *17*, 566. [CrossRef]
30. Holmgren, W.F.; Hansen, C.W.; Mikofski, M.A. pvlib python: A python package for modeling solar energy systems. *J. Open Source Softw.* **2018**, *3*, 884. [CrossRef]

31. King, D.L.; Kratochvil, J.A.; Boyson, W.E. Temperature coefficients for PV modules and arrays: Measurement methods, difficulties, and results. In Proceedings of the Conference Record of the Twenty Sixth IEEE Photovoltaic Specialists Conference, Anaheim, CA, USA, 29 September–3 October 1997; pp. 1183–1186.
32. Solís-Alemán, E.M.; de la Casa, J.; Romero-Fiances, I.; Silva, J.P.; Nofuentes, G. A study on the degradation rates and the linearity of the performance decline of various thin film PV technologies. *Sol. Energy* **2019**, *188*, 813–824. [CrossRef]
33. Kichou, S.; Abaslioglu, E.; Silvestre, S.; Nofuentes, G.; Torres-Ramírez, M.; Chouder, A. Study of degradation and evaluation of model parameters of micromorph silicon photovoltaic modules under outdoor long term exposure in Jaén, Spain. *Energy Convers. Manag.* **2016**, *120*, 109–119. [CrossRef]
34. Mikofski, M.A. polyfitZero Version 1.3.0.0. MATLAB Central File Exchange. Available online: https://www.mathworks.com/matlabcentral/fileexchange/35401-polyfitzero (accessed on 15 October 2024).
35. Gulkowski, S. Modeling and Experimental Studies of the Photovoltaic System Performance in Climate Conditions of Poland. *Energies* **2023**, *16*, 7017. [CrossRef]
36. Eke, R.; Demircan, H. Performance analysis of a multi crystalline Si photovoltaic module under Mugla climatic conditions in Turkey. *Energy Convers. Manag.* **2013**, *65*, 580–586. [CrossRef]
37. Drouiche, I.; Harrouni, S.; Arab, A.H. A new approach for modelling the aging PV module upon experimental I–V curves by combining translation method and five-parameters model. *Electr. Power Syst. Res.* **2018**, *163*, 231–241. [CrossRef]
38. Senturk, A. Investigation of datasheet provided temperature coefficients of photovoltaic modules under various sky profiles at the field by applying a new validation procedure. *Renew. Energy* **2020**, *152*, 644–652. [CrossRef]
39. Osterwald, C.R. Translation of device performance measurements to reference conditions. *Solar Cells* **1986**, *18*, 269–279. [CrossRef]
40. Muñoz-García, M.A.; Marin, O.; Alonso-García, M.C.; Chenlo, F. Characterization of thin film PV modules under standard test conditions: Results of indoor and outdoor measurements and the effects of sunlight exposure. *Sol. Energy* **2012**, *86*, 3049–3056. [CrossRef]
41. Dolara, A.; Cabrera-Tobar, A.; Ogliari, E.; Leva, S.; Hanne, L. Design of an Embedded Test Bench for Organic Photovoltaic Module Testing. *Electronics* **2024**, *13*, 3104. [CrossRef]
42. Gulkowski, S.; Muñoz Diez, J.V.; Aguilera Tejero, J.; Nofuentes, G. Computational modeling and experimental analysis of heterojunction with intrinsic thin-layer photovoltaic module under different environmental conditions. *Energy* **2019**, *172*, 380–390. [CrossRef]
43. Adigüzel, E.; Gürkan, K.; Ersoy, A. Design and development of data acquisition system (DAS) for panel characterization in PV energy systems. *Measurement* **2023**, *221*, 113425. [CrossRef]

Disclaimer/Publisher's Note: The statements, opinions and data contained in all publications are solely those of the individual author(s) and contributor(s) and not of MDPI and/or the editor(s). MDPI and/or the editor(s) disclaim responsibility for any injury to people or property resulting from any ideas, methods, instructions or products referred to in the content.